



Ultra-SAXS observation of fibril-sized structure formation after the necking of poly(ethylene terephthalate) and poly(phenylene sulfide) fibers

Ren Tomisawa¹ · Takumi Ando¹ · Toshifumi Ikaga¹ · Kyoungou Kim¹ · Yutaka Ohkoshi^{1,2} · Kazuyuki Okada³ · Hiroyasu Masunaga⁴ · Toshiji Kanaya⁵ · Hiroo Katsuta⁶ · Yoshitsugu Funatsu⁶

Received: 31 July 2018 / Revised: 4 October 2018 / Accepted: 5 October 2018 / Published online: 9 November 2018
© The Society of Polymer Science, Japan 2018

Abstract

Fibril-sized structures, which exhibit a density fluctuation of several tens to hundreds of nanometers, are important because they influence many properties of fibers and films, particularly the strength and thermal shrinkage of synthetic fibers. We analyzed the formation of fibril-sized structures after necking using ultra-small-angle X-ray scattering (USAXS), which enables observation of the void and craze formations. Continuous laser-heated drawing and undulator synchrotron radiation were adopted to measure the structural development of poly(ethylene terephthalate) (PET) and poly(phenylene sulfide) (PPS) fibers. Both fibers showed a clear increase in the meridional streak intensity just after necking and an increase in the equatorial streak after necking. These increases were distinctive for PPS. Moreover, a layer-lined streak appeared after necking only for PET. The intensity of the meridional streak increased with an increase in the draw ratio, whereas the intensity of the layer-lined scattering decreased with an increase in the draw ratio.

Introduction

It is known that the strength and Young's modulus of synthetic fibers are greatly improved by orientation-induced crystallization during spinning and drawing. However, the strengths of the obtained fibers are only a few percent of the theoretical strength of perfect crystals [1]. This is mainly because large amorphous regions remain in the fine structure of the fiber and the structure is nonuniform. According to the weak-link theory [2], for brittle materials, the failure generally depends on the strength of the weakest part. However, for ductile polymeric materials, the strength is not determined only by weak points; that is, the defects are

propagated in the fiber structure by the drawing, and thus, the strength is determined by the degree of dispersion of the weak points.

In discussing the uniformity of entanglement structures, it is essential to understand the internal hierarchical structure of synthetic fibers. In the hierarchical structure of synthetic fibers, structures on the scale of several nanometers (microfibril structures) [3–5] are observed within structures on the scale of several hundred nanometers (macrofibril structures) [5–7]. The weakest point of the structure is probably caused by the interface of this hierarchical structure, and thus, the fiber strength can be improved by increasing the uniformity of the hierarchical fibrillar structure.

✉ Kyoungou Kim
Khkim@shinshu-u.ac.jp

¹ Faculty of Textile Science and Technology, Shinshu University, 3-15-1 Tokida, Ueda, Nagano 386-8567, Japan

² Division of Frontier Fibers, Institute for Fiber Engineering, Shinshu University, 3-15-1 Tokida Ueda, Nagano Prefecture 386-8567, Japan

³ Material Science Laboratories, Toray Research Center Inc., 3-3-7

Sonoyama, Otsu, Shiga 520-8567, Japan

⁴ Japan Synchrotron Radiation Research Institute, 1-1-1 Kouto, Sayo-cho, Sayo-gun, Hyogo 679-5148, Japan

⁵ High Energy Accelerator Research Organization, 203-1 Shirakata, Tokai-mura, Naka-gun, Ibaraki 319-1106, Japan

⁶ Fibers and Textiles Research Laboratories, Toray, 4845 Mishima, Shizuoka 411-8652, Japan

The typical fiber structure development of poly(ethylene terephthalate) (PET), that is, the structure formation that occurs during spinning and drawing, has been intensely researched. Kolb et al. [8] measured the orientation-induced crystallization with a time resolution of 0.3–0.6 ms in the high-speed spinning of PET fibers taken up at 4000 m/min. Mahendrasingam et al. [9] and Kawakami et al. [10] studied the structural change that occurred during batch drawing of a PET film. More recently, Okada et al. [11] obtained X-ray images in the through and edge directions of a uniaxially drawn PET film and investigated the differences in the structural changes in each direction. In the edge image, shear deformation was observed as a shear band-like structure formed by stacking benzene rings. Yamaguchi et al. [12] also observed a fibrillar smectic structure of several nanometers in diameter and several tens of nanometers in length within 1 ms after drawing, which was a long-period structure of approximately 4–5 periods. This smectic structure was considered to be the precursor of a microfibrillar structure. From our previous research [13], coupled with that of Yamaguchi, the amounts of smectic phase and d-spacing during the drawing of PET fibers were analyzed in more detail. As a result, the fiber strength was observed to be determined by the amount and orientation of the intermicrofibrillar tie-chains linking the smectic phase, not the microfibrillar structure itself. Therefore, it is important for the fiber strength that the entangled network of molecular chains bears the strength efficiently. However, these studies only focused on the several nanometer-scale structures, and the influence of microfibrils and shear bands on the uniformity of fibrils was not examined.

The structure and properties of poly(phenylene sulfide) (PPS) have also been studied [14–18]. PPS can easily form a rigid amorphous phase [19] because of its rigid molecular chain compared with that of PET, and there is little difference between the crystal and amorphous regions. The fiber structure model of PPS was proposed by Perret et al. [18]. Recently, Ide et al. revealed the fiber structure development process during the drawing of PPS fibers [20], and it was reported that PPS forms orthorhombic crystals through the pseudo-hexagonal mesophase. The X-pattern appeared at the initial stage of structure formation in small-angle X-ray scattering (SAXS), and it changed to the four-point pattern with elapsed time. However, the analysis of structures on the scale of several tens to hundreds of nanometers is still lacking. In this study, we attempted to obtain an ultra-SAXS (USAXS) image of the continuous drawing of the PET and PPS fibers. A very strong X-ray beam generated by synchrotron radiation equipped with an undulator was used for the measurement. The fibrillar structure, which was several tens to hundreds of nanometers in diameter, was analyzed by the USAXS images.

Experimental

Sample

The fibers used for drawing were prepared by melt-spinning of PET ($IV = 1.32 \text{ dL/g}$) and PPS ($MFR = 120 \text{ g/10 min}$) provided by the Toray Co. The PET polymer was heated at $300 \text{ }^\circ\text{C}$, and the PPS polymer was heated at $330 \text{ }^\circ\text{C}$. Both polymers were extruded from a one-hole nozzle at a mass flow rate of 5.0 g/min and taken up at 250 m/min . The nozzle diameter was 1.0 mm , and the length-to-diameter ratio was 3.

Drawing

The fibers were fed continuously from a feed roller, heated by irradiation with a CO_2 laser beam, and drawn based on the speed difference between the feed and take-up rollers [12]. The fiber running speed after necking was fixed at 110 m/min , and the draw ratio (DR) was changed by changing the feeding speed. A random polarized laser beam with a wavelength and diameter of $10.6 \mu\text{m}$ and 6 mm , respectively, was generated using a PIN-30R laser (Onizuka Glass Co., Ltd.). The beam was used to irradiate the running fibers from three different directions. The laser power for each drawing condition was determined to enable fluctuations in the neck-drawing point to be minimized. The drawing tension was measured using a tension meter (HS-1500S, Eiko Sokki Co., Ltd.). A 100 gf pickup was installed between the neck-drawing point and the take-up roller. The drawing stress was calculated from the drawing tension and the diameter of the drawn fiber. The drawing conditions are shown in Table 1.

On-line measurement

USAXS images were obtained by X-ray irradiation of the running fiber during the continuous drawing. The on-line measurement system has been described in a previous report [12]. The distance from the necking point to the X-ray irradiation position was changed by moving the laser irradiation position. The elapsed time after necking was calculated by dividing the distance by the fiber running speed.

The distance between the necking point and the X-ray irradiation position was measured with a CCD video camera (Watec Co., Ltd. WAT-232S type) that was placed coaxial to the X-ray beam using a mirror. The CCD video camera was equipped with a telecentric lens (OPTART Co., Ltd. TV-2S) with double magnification. The synchrotron X-ray beam used in this study was from SPring-8 BL03XU (FSBL), and an undulator was used to obtain an ultrahigh-intensity X-ray beam. The X-ray beam diameter was $10 \mu\text{m}$, which was obtained through a $9 \mu\text{m}$ defining pinhole

Table 1 Structure and physical properties of the drawn fibers

Sample	Draw ratio	Drawing stress, MPa	Birefringence	Tensile strength, MPa	Elongation, %	Young's modulus, GPa	Thermal shrinkage, %	Melting temperature, °C	Heat of fusion, J/g	Crystallinity, %
PET	4.4	61	0.165	759	50	9.7	16	254	46	34
	5.0	105	0.179	944	33	10.9	19	255	52	38
	5.6	188	0.193	1087	26	10.8	20	256	53	40
PPS	4.3	100	–	677	24	6.4	14	283	40	28

(50 mm-thick tantalum). Two pairs of Si crystals were arranged immediately downstream of the pinhole. The Si crystals were arranged vertically and horizontally under conditions that satisfy Bragg's diffraction angle. The parasitic scattering emitted from the defining pinhole was removed by the Si crystals. The Pilatus detector (DECTRIS Co. Pilatus3 S 1M), which has 1043×981 pixels ($172 \mu\text{m}/\text{pixel}$), was also used. The wavelength of the X-ray beam was 0.155 nm, the camera length was 7564 mm, and the exposure time was 60 s.

The time resolution was calculated using the same calculation method as previously reported [20]. Image processing could not be performed because the image extracted from the necking movie in this experiment was rough and blurred. Therefore, the time resolution was estimated by the length and the fluctuations of the necking with reference to those previously reported [13, 20]. That is, it was estimated that the neck fluctuation was 0.09–0.14 mm and the neck length was 0.13–0.28 mm for PET fibers, and the neck fluctuation was 0.095 mm and the necking length was 0.06 mm for PPS; the size of the X-ray beam was 0.01 mm, and the fiber running speed was 110 m/min. The estimated time resolution was 0.09–0.17 ms for PET and 0.06 ms for PPS.

Birefringence

The birefringence for each fiber was measured by a polarized light microscope (BX51-33POC, Olympus Co., Ltd.) with a monochromic filter of 546 nm. Tricresyl phosphate was used as an immersion oil. The average and standard deviation of birefringence were calculated for 10 samples.

Physical properties test

The thermal and mechanical properties of the drawn fibers were analyzed by tensile tests, thermomechanical analysis (TMA), and differential scanning calorimetry (DSC). The strength, elongation, and Young's modulus were measured by a universal testing machine (Autograph AGS-X, Shimadzu Co. Ltd.) equipped with a 50 N load cell and air chuck. The sample length and elongation rate were 40 mm and 100%/min, respectively, and the average and standard

deviations of the strength, elongation, and Young's modulus were calculated for every 10 samples.

A thermomechanical analyzer (TMA/SS6100, SII Nanotechnology Inc.) was used to measure the thermal shrinkage factor and the shrinkage stress at heating rates of 5 and 10 K/min, respectively. The sample length was 10 mm for both measurements. DSC was conducted using a calorimeter (Thermoplus DSC8230, Rigaku Co. Ltd.) with a heating rate of 10 K/min. Powder cut fibers were used for the sample of DSC measurements.

Results and discussion

Properties and structures of fibers

The structure and properties of the PET and PPS fibers are shown in Table 1. The birefringence of the as-spun fibers was very small, approximately 0.0001, because both fibers were spun at the lowest speed at which stable winding could be achieved. The birefringence and tensile strength were increased, while the elongation was decreased with the increase of the drawing stress for the PET fibers. It was considered that the larger drawing stress applied to the fiber oriented the molecular chains to the fiber axis and increased the fiber strength.

Neck drawing and fiber temperature

As seen in Table 1, PET was drawn with DRs of 4.4, 5.0, and 5.6, and PPS was drawn with a DR of 4.3. The drawing stress was 61–188 MPa for PET and 100 MPa for PPS. PPS could be drawn in an extremely narrow drawable range of 4.2–4.4 and thus was measured only with a draw ratio of 4.3.

The fiber temperatures around the necking point were estimated. The estimated profile was obtained on the basis of an energy balance equation considering the temperature rise by laser irradiation, cooling by heat transfer from the fiber surface, the work of plastic deformation by an external force, and the latent heat of crystallization [21]. The heat of crystallization was determined using the heat of fusion of the drawn fibers measured by DSC (Table 1). The crystallization induction time and crystallization rate were

Table 2 Fiber temperatures estimated for the drawing conditions

Sample	Draw ratio	Crystallization induction time, ms	Crystallization rate, $\times 10^3/s$	Temperature immediately before the neck, °C	Temperature immediately after the neck, °C	Max. temp. and time, °C(ms)
PET	4.4			83	109	152 (2.4)
	5.0	0.6 ^a	2.3 ^a	100	140	185 (2.3)
	5.6			109	180	222 (2.4)
PPS	4.3	0.02	3	76	119	163 (2.0)

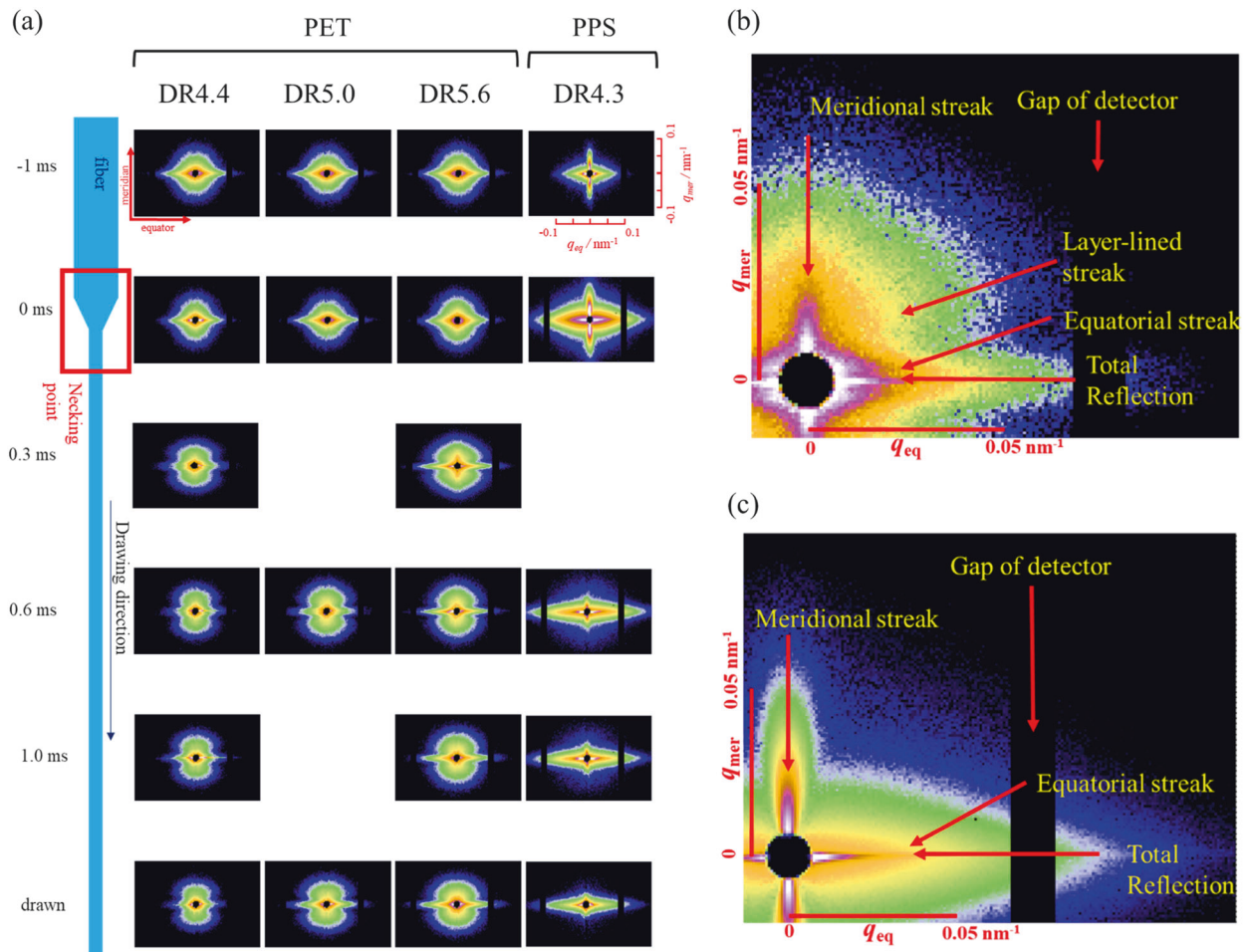
^aAssumed value

Fig. 1 **a** USAXS images of PET and PPS fibers at corresponding elapsed times after necking. The elapsed times after necking are noted in the images. Typical USAXS images of **b** a PET fiber with DR 5.6 at

0.1 ms and **c** PPS fiber with DR 4.3 at 0 ms after necking. q_{eq} and q_{mer} are the scattering vectors along the equatorial and meridional directions, respectively

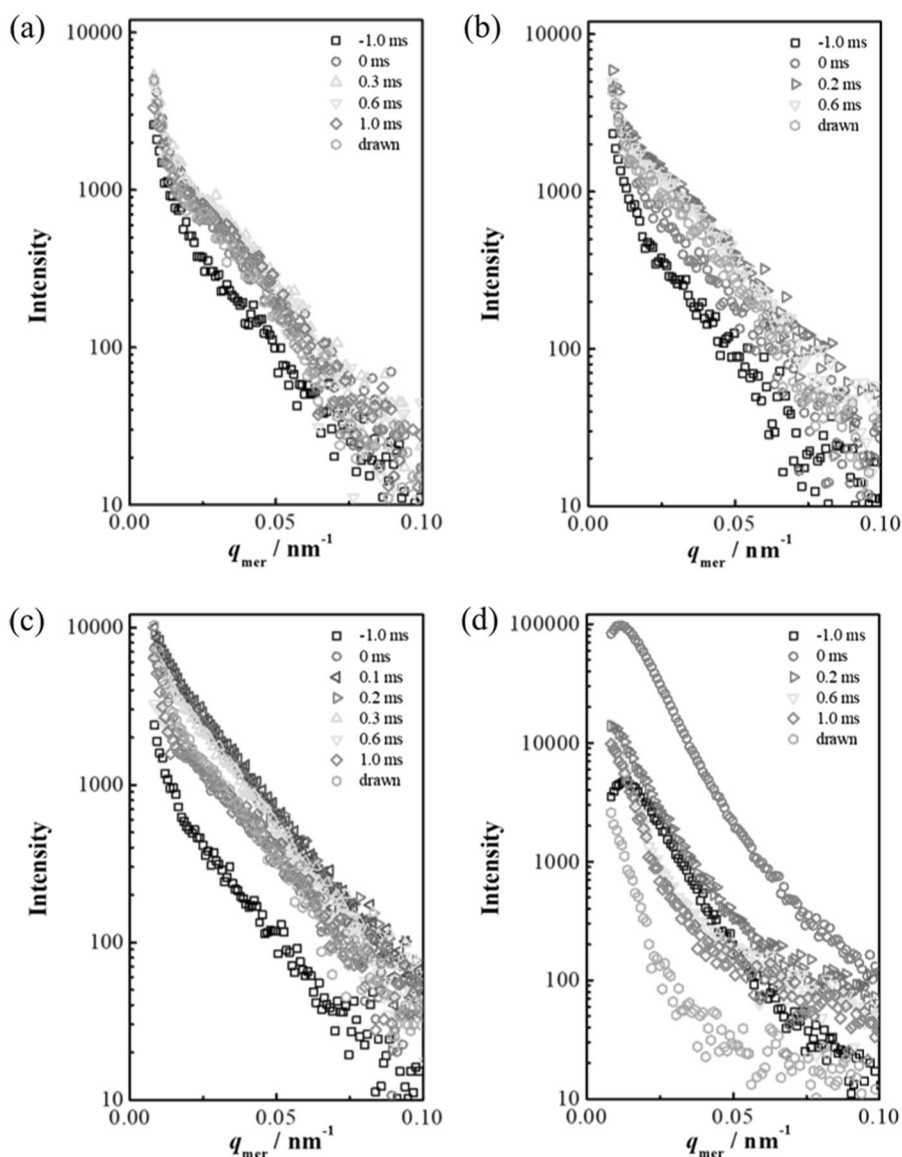
assumed, as shown in Table 2, with reference to the results of a previous report [13] and the value obtained by Ide et al. [20]. The estimated fiber temperature is shown in Table 2.

USAXS pattern

The USAXS images obtained by subtracting air scattering are shown in Fig. 1. Figure 1a shows the scattering patterns

of each elapsed time and draw ratio, and Fig. 1b, c shows the typical USAXS scattering patterns for PET and PPS. The horizontal direction of the figure shows the equatorial direction, and the vertical direction shows the meridional direction. As shown in Fig. 1c, three streaks were observed for the USAXS pattern of PPS, which were the meridional and equatorial streaks and the total reflection. In addition to the three streaks observed for PPS, a layer-lined streak was

Fig. 2 Meridional intensity profiles. **a** PET, DR 4.4; **b** PET, DR 5.0; **c** PET, DR 5.6; and **d** PPS DR 4.3. Elapsed times are noted in the profiles



observed for PET (Fig. 1b). The extremely strong and thin streak overlapped with the streak of the fibril-sized structure in the equatorial direction. This should be the total reflection from the fiber surface. The total reflection could be cut off greatly by made a thinner X-ray beam. Although an X-ray beam approximately 1/6 of the fiber diameter was used in this study, we could not completely prevent the total reflection because the fiber fluctuated slightly along the perpendicular direction to the fiber axis. However, the total reflection could be distinguished clearly from the equatorial scattering because it was so sharp. Its influence was limited to a very narrow range around the equator.

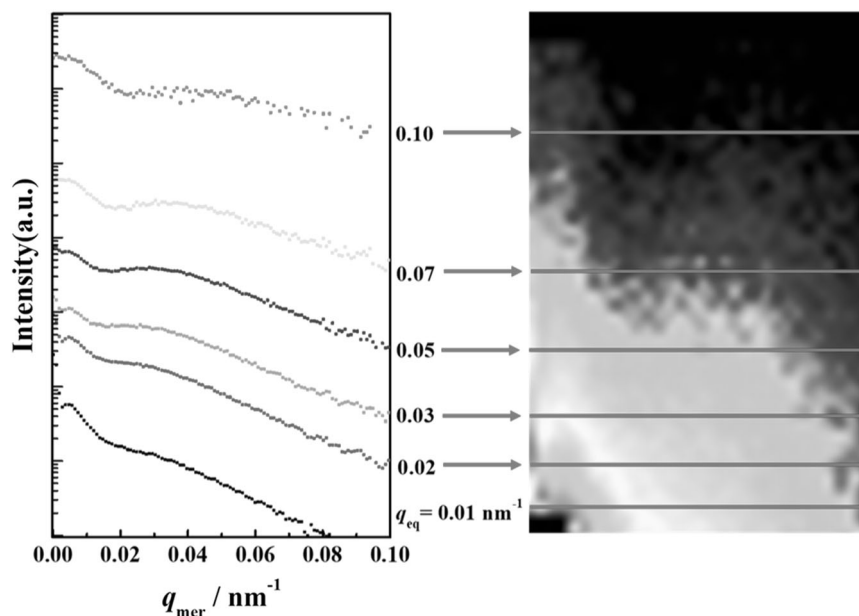
Figure 1a shows the USAXS pattern changing with the elapsed time. The negative elapsed time represents the data

before necking, and 0 ms denotes the image taken at the necking point. Before necking, meridional and equatorial streaks were observed for PPS, while an equatorial streak was observed for the as-spun PET fiber. Upon necking, both equatorial and meridional streak intensities greatly increased. A layer-lined streak and a meridional streak also appeared. However, the layer-lined streak for DR 5.6 was unclear. Afterwards, the meridional streak was weakened with elapsed time.

Meridional streak

The meridional intensity profile of the USAXS image is shown in Fig. 2. The measured range of the scattering vector q from 0.007 to 0.15 nm^{-1} corresponds to a

Fig. 3 Intensity profiles along the meridional direction at each q_{eq} obtained by a drawn PET fiber with DR 4.4 at 0.3 ms after necking. The q_{eq} are noted in the profiles



scattering body size of 50–900 nm. A meridional peak at q_{mer} of 0.012 nm^{-1} was observed only for PPS at -1.0 to 0 ms and disappeared after necking. The corresponding size of the period was approximately 500 nm. For both PET and PPS, the intensity of the meridional streak reached a maximum immediately after necking. The maximum intensity for PPS was more than ten times larger than that of PET, and the intensity increased with the drawing stress for PET. Afterward, the intensity decreased with the elapsed time for both PET and PPS. However, the streak intensity of the drawn PET fiber was still larger than that for the as-spun PET fiber, while the intensity of the drawn PPS fiber became smaller than that before drawing. Furthermore, a broad shoulder appeared around $q_{\text{mer}} = 0.03 \text{ nm}^{-1}$ at DRs 4.4 and 5.0 for PET, while this was not observed for DR 5.6. The corresponding size of the shoulder was approximately 200 nm.

The meridional peak observed at -1.0 ms showed a periodic density fluctuation along the fiber axis in the as-spun PPS fiber. The density fluctuation amplified by the necking was thought to arise from the craze formed in the lower-density region. The elongational deformation of necking should form a craze, and the weakening of the meridional streak indicates collapse of the craze. The larger intensity increase in PPS, indicating a larger degree of craze formation, should be caused by the density fluctuation already occurring in the as-spun fiber.

Layer-lined streak and equatorial streak

To analyze these equatorial and layer-lined streaks, the USAXS image was analyzed as follows. Figure 3 shows the intensity profiles along the meridional direction (q_{mer}).

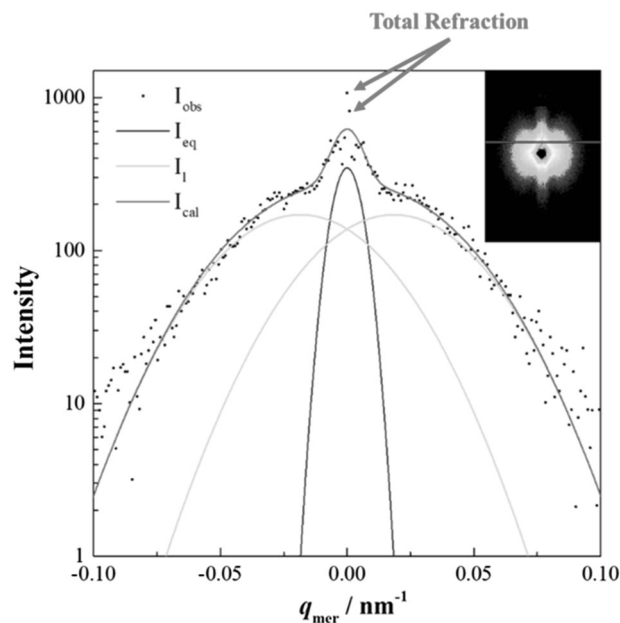
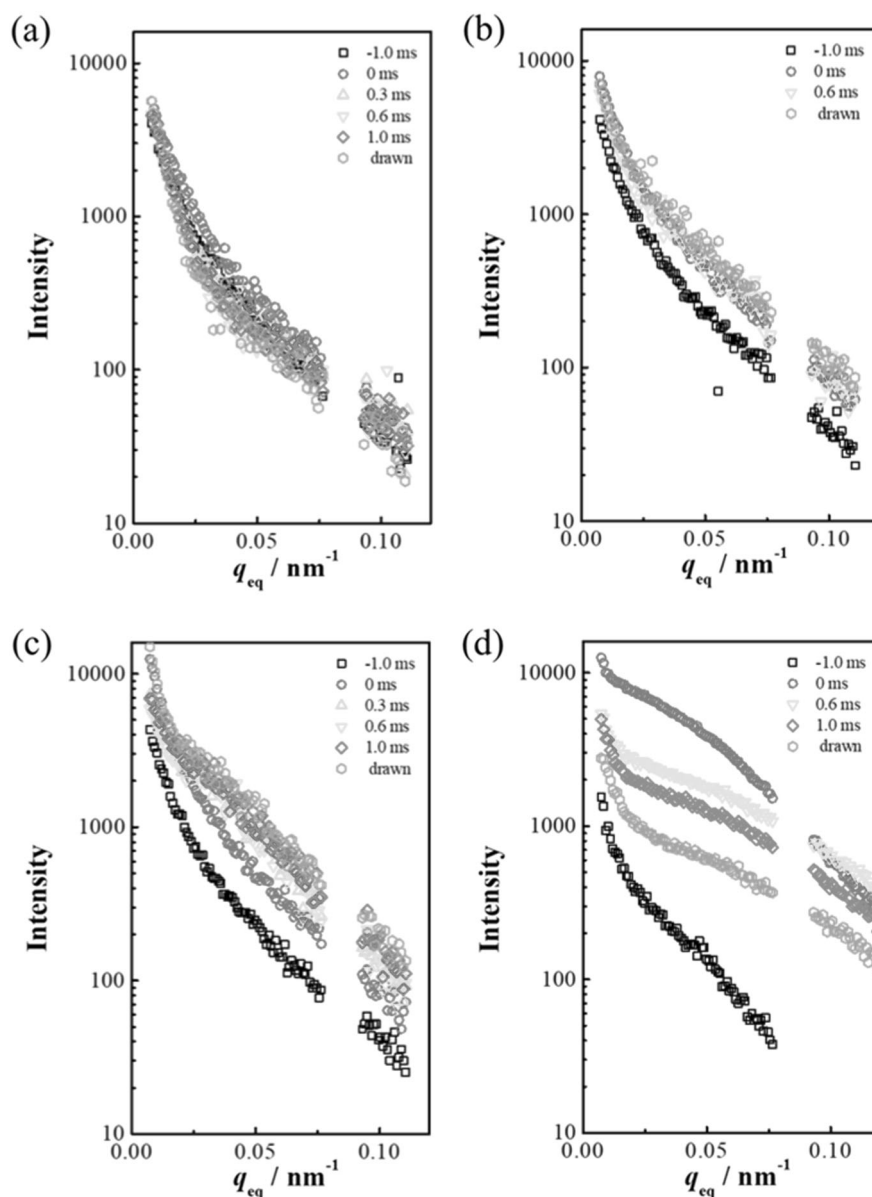


Fig. 4 An example of peak fitting for a PET fiber drawn 4.4 times at 0.3 ms after necking. The intensity profile along the meridian direction at $q_{\text{eq}} = 0.023$ was fitted by Gaussian equatorial scattering (I_{eq}) and symmetrical layer-lined scattering (I_l) after deleting the total reflection influenced data

When q_{mer} exceeded 0.02 nm^{-1} , the peak of the layer-lined streak could be distinguished from the equatorial peak. To separate the components of the equatorial streak and layer-lined streak, the intensity profile was fitted by a Gaussian function, as shown in Fig. 4. The layer-lined streak was assumed to be symmetrical to the equatorial axis. Prior to the peak fitting, we deleted several data to eliminate the total reflection. Because the total reflection was far sharper

Fig. 5 Equatorial intensity profiles obtained from peak fitting, similar to Fig. 3. **a** PET, DR 4.4; **b** PET, DR 5.0; **c** PET, DR 5.6; and **d** PPS DR 4.3. Elapsed times are noted in the profiles



than the equatorial streak, it could be ignored except for the very narrow range of q_{mer} . The deleted data range was $|q_{\text{mer}}| < 0.0037 \text{ nm}^{-1}$ for PET, and $|q_{\text{mer}}| < 0.0055 \text{ nm}^{-1}$ for PPS.

The equatorial profiles obtained by the fitting are shown in Fig. 5. For PET with DR 4.4, the intensity profile of the equatorial streak did not change substantially over time, while the intensity clearly increased as a result of necking for the larger draw ratios. In addition, as it is clearly shown for DR 5.6, the intensity continued to increase and tended to saturate at 1.0 ms. In contrast, for PPS, the intensity was drastically increased as a result of necking and decreased with the elapsed time. The intensity increase due to necking was far larger than the increase observed for PET.

The equatorial streak indicated a density fluctuation of several hundred nanometers perpendicular to the fiber axis,

which seemed to be the density difference between the so-called fibril and interfibrillar void. The larger increase in the streak intensity observed for PPS and the higher-ratio-drawn PET seemed to indicate the formation of more interfibrillar voids. In contrast, the intensity decrease should indicate the dissipation of the voids. The large decrease in the PPS intensity seemed to be caused by the dissipation of interfibrillar voids formed by necking. However, although the interfibrillar voids should also collapse with elapsed time for PET, they increased with time, particularly for DR 5.6. This could be explained by the voids formed by crystallization, which occurred less than 1.0 ms after necking [13].

The position of the layer-lined peak along q_{mer} was plotted against q_{eq} (Fig. 6). The streak appeared immediately after necking, and its position hardly changed with

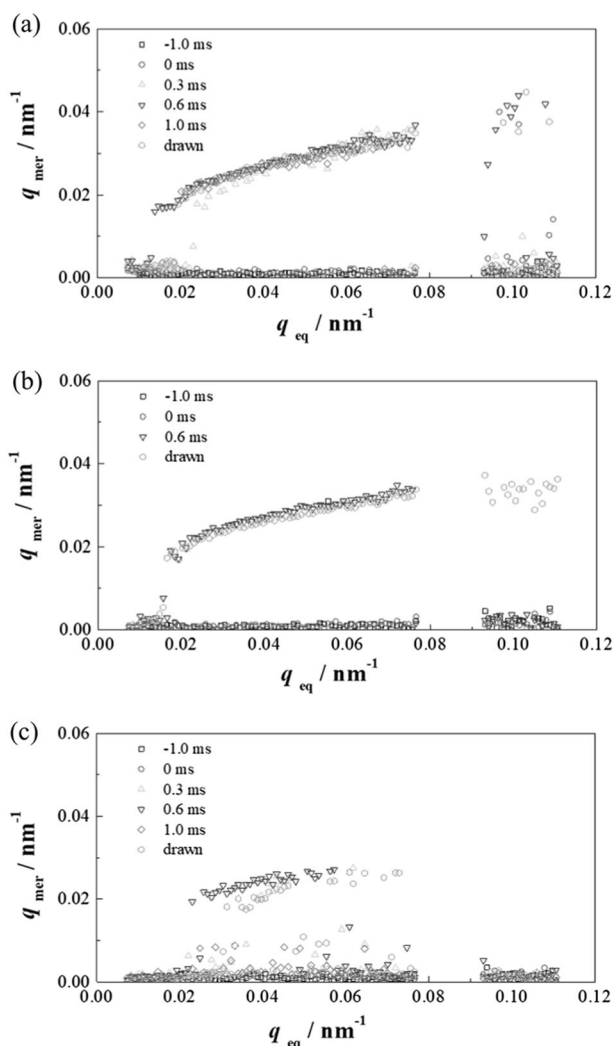


Fig. 6 Peak position of the layer-lined streak. Draw ratio: **a** 4.4, **b** 5.0, and **c** 5.6. Elapsed times are noted in the images

elapsed time. The position also hardly changed with the draw ratio, but the peak separation became difficult owing to the decrease in the streak intensity, particularly at low q_{eq} . The position of the peak was inclined approximately 20° from the equator, which was similar to the inclination of the X-pattern observed for SAXS [13]. Therefore, it should not be a simple layer-lined streak, but it can be thought of as a meridional shoulder peak observed at approximately $q_{mer} = 0.03 \text{ nm}^{-1}$ and overlapped with the X-shaped streak.

Fibril-size structure development of PET and PPS

It is interesting that the USAXS patterns of PET and PPS were different although their SAXS patterns were similar. That is, both showed an X-shaped SAXS streak changing to a four-point pattern [13, 20]. However, only PET showed the layer-lined USAXS streak, and PPS showed a far stronger USAXS meridional streak than PET. The

layer-lined USAXS streak of PET can be explained by the fibrillar-shaped smectic phase that formed less than 1.0 ms after necking and then grew to a microfibril [12]. This smectic phase is a metastable structure, first reported by Bonart [22], that has been formed during the batch drawing [11] and heat treatment of oriented amorphous PET [23]. The smectic phase has also been observed for PEN [24] and PBT [25], although it has not been observed for PPS [20]. The period of 200 nm, corresponding to the layer-lined USAXS streak, can be assumed to be the period of a layered bundle of a fibrillar-shaped smectic phase of approximately 70 nm in length [12] and interfibrillar molecules. A far stronger meridional streak of PPS should be caused by the periodic density deviation formed preliminarily in the as-spun fiber. Because of the density deviation along the fiber axis, craze formation preferentially occurred by necking for PPS, whereas slippage between the fibril-forming molecules preferentially occurred in the PET.

Conclusions

We analyzed the formation of fibril-sized structures after necking using USAXS, which enables observation of void and craze formations. Continuous laser-heated drawing and undulator synchrotron radiation were adopted to measure the structural development of PET and PPS fibers. PET was drawn with DRs of 4.4, 5.0, and 5.6, and PPS was drawn with a DR of 4.3. The drawing stress was 61–188 MPa for PET and 100 MPa for PPS.

Three streaks were observed for the USAXS pattern of PPS, which were meridional and equatorial streaks and the total reflection. In addition to the three streaks observed for PPS, a layer-lined streak was observed for PET. A meridional peak corresponding to an approximately 500 nm period was observed only for PPS before necking. Both fibers showed a clear increase in the meridional streak intensity just after necking and an increase in the equatorial streak after necking. These increases were distinctive for PPS. Moreover, a layer-lined streak appeared after necking only for PET. The intensity of the meridional streak increased with an increase in the draw ratio, whereas the intensity of layer-lined scattering decreased with an increase in the draw ratio.

The far stronger meridional streak of PPS may be caused by the periodic density deviation formed preliminarily in the as-spun fiber, and the layer-lined USAXS streak of PET can be explained by the periodic bundle of a fibrillar-shaped smectic phase.

Acknowledgments This study was supported by Grants-in-Aid for Scientific Research (Nos. 17K05990 and 16K05910) from the Ministry of Education, Culture, Sports, Science and Technology (MEXT), Japan. Experiments were performed at the SPring-8 synchrotron radiation facility (No. 2016A7213). We thank the

Edanz Group (www.edanzediting.com/ac) for editing a draft of this manuscript.

Compliance with ethical standards

Conflict of Interest The authors declare no conflict of interest.

References

1. Kikutani T, Masubuchi Y, Sakurai S, Murase H, Ohkoshi Y, Shioya M et al. Fundamental and Practical Technologies for Nano-Structured Polymeric Materials”, CMC Press, Tokyo, CMC Publishing Co., Ltd. ISBN978-4-7813-0043-6, (2008), p. 56–110.
2. Nitta K. *Kobunshi Ronbunshu*. 2016;73:281–93.
3. Reneker DH, Geil PM. *J Appl Phys*. 1960;31:1916.
4. Yamaguchi S, Tatemoto. M, Tsuji M. *Kobunshi Ronbunshu*. 1990;47:105–8.
5. Nakamae K, Kotera M, Iino K. *Sen'i Gakkaishi*. 2002;58:99–102.
6. Abe Y, Sakamoto R. *Kobunshi Ronbunshu*. 1976;33:263–9.
7. Shimamura K, Murakami S, Tsuji M, Katayama K. *Nihon Reoroji Gakkaishi*. 1979;7:42–46.
8. Kolb R, Seifert S, Stribeck N, Zachmann HG. *Polymer*. 2000; 41:2931.
9. Mahendrasingam A, Martin C, Fuller W, Blundell DJ, Oldman RJ, MacKerron DH, et al. *Polymer*. 2000;41:1217.
10. Kawakami D, Hsiao BS, Burger C, Ran S, Avila-Orta C, Sics I, et al. *Macromolecules*. 2005;38:91.
11. Okada K, Nakata K, Higashioji Y, Takahashi K, Ohkoshi Y, Kanaya T. *Kobunshi Ronbunshu*. 2014;71:593–600.
12. Yamaguchi T, Kim KH, Murata T, Koide M, Hitoosa S, Urakawa H, et al. *J Polym Sci Polym Phys*. 2008;46:2126–42.
13. Tomisawa R, Ikaga T, Kim KH, Ohkoshi Y, Okada K, Masunaga H, et al. *Polymer*. 2017;116C:357–66.
14. Houis S, Schmid M, Lubben J.J *Appl Polym Sci*. 2007;106:1757.
15. Gulgunje P, Bhat G, Spruiell J.J *Appl Polym Sci*. 2011;122: 3110.
16. Gulgunje P, Bhat G, Spruiell J.J *Appl Polym Sci*. 2012;125:1890.
17. Gulgunje P, Bhat G, Spruiell J.J *Appl Polym Sci*. Part 3. 2012;125:1693.
18. Perret E, Reifler FA, Hufenus R, Bunk O, Heuberger M. *Macromolecules*. 2013;46:440. 15
19. Huo P, Cebe P. *Colloid Polym Sci*. 1992;270:840.
20. Ide K, Ikaga T, Ohkoshi Y, Wataoka I, Masuda M, Maeda Y. *Sen'i Gakkaishi*. 2014;70:4.
21. Okumura W, Yamaguchi T, Ohkoshi Y, Gotoh Y, Nagura M. *Intern Polym Proc*. 2002;17:124–32.
22. Bonart R. *Kolloid Z*. 1966;213:1–11.
23. Asano T, Balta Calleja FJ, Flores A, Tanigaki M, Mina M, Sawatari C, et al. *Polymer*. 1999;40:6475–84.
24. Kim KH, Aida R, Kang YA, Ikaga T, Ohkoshi Y, Wataoka I, et al. *Polymer*. 2012;53:4272–9.
25. Konishi T, Miyamoto Y. *Polymer*. 2010;42:349–53.